

# Structural and Magnetic Properties of LaCoO<sub>3</sub>/SrTiO<sub>3</sub> Multilayers

Hongrui Zhang,<sup>†</sup> Jing Zhang,<sup>†</sup> Huaiwen Yang,<sup>†</sup> Qianqian Lan,<sup>†</sup> Deshun Hong,<sup>†</sup> Shufang Wang,<sup>‡</sup> Xi Shen,<sup>†</sup> Tahira Khan,<sup>†</sup> Richeng Yu,<sup>†</sup> Jirong Sun,<sup>\*,†</sup> and Baogen Shen<sup>†</sup>

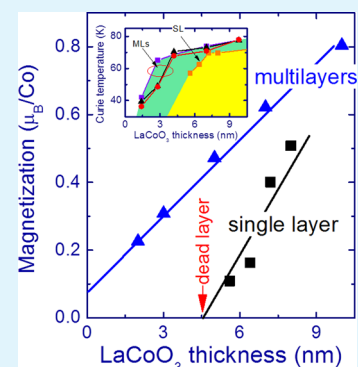
<sup>†</sup>Beijing National Laboratory for Condensed Matter & Institute of Physics, Chinese Academy of Sciences, Beijing 100190, People's Republic of China

<sup>‡</sup>College of Physics Science and Technology, Hebei University, Baoding 071002, Hebei Province, People's Republic of China

## Supporting Information

**ABSTRACT:** Structural and magnetic properties of the LaCoO<sub>3</sub>/SrTiO<sub>3</sub> (LCO/STO) multilayers (MLs) with a fixed STO layer of 4 nm but varied LCO layer thicknesses have been systematically studied. The MLs grown on Sr<sub>0.7</sub>La<sub>0.3</sub>Al<sub>0.65</sub>Ta<sub>0.35</sub>O<sub>3</sub> (LSAT) and SrTiO<sub>3</sub> (STO) exhibit the in-plane lattice constant of the substrates, but those on LaAlO<sub>3</sub> (LAO) show the in-plane lattice constant between those of the first two kinds of MLs. Compared with the LCO single layer (SL), the magnetic order of the MLs is significantly enhanced, as demonstrated by a very slow decrease, which is fast for the SL, of the Curie temperature and the saturation magnetization as the LCO layer thickness decreases. For example, clear ferromagnetic order is observed in the ML with the LCO layer of ~1.5 nm, whereas it vanishes below ~6 nm for the LCO SL. This result is consistent with the observation that the dark stripes, which are believed to be closely related to the magnetic order, remain clear in the MLs while they are vague in the corresponding LCO SL. The present work suggests a novel route to tune the magnetism of perovskite oxide films.

**KEYWORDS:** multilayers, perovskite oxides, interlayer coupling, HAADF image, ferromagnetic order, magnetic dead layer



## 1. INTRODUCTION

Epitaxial strain in perovskite oxide thin films induced by film–substrate lattice mismatch can affect many physical properties, such as electronic structure, conductivity, magnetism, and ferroelectricity.<sup>1–5</sup> In particular, unexpected physical phenomena which are absent in bulk counterparts can be induced by lattice strain in thin films. LaCoO<sub>3</sub> (LCO) is an interesting perovskite oxide, for which tensile strains cause a ferromagnetic (FM) order below ~80 K<sup>6–9</sup> though bulk LCO is nonmagnetic at low temperatures.<sup>10–13</sup> As well documented, the spin state of Co<sup>3+</sup> ions is susceptible to structural deformation because of the similar energies of crystal-field splitting and Hund's coupling, and tensile strain causes a low-spin (LS) to high-spin (HS) state transition for parts of the Co<sup>3+</sup> ions. By adjusting the degree of the tensile strains of the LCO films, both the Curie temperature ( $T_C$ ) and the saturation magnetization ( $M_S$ ) can be tuned in a wide range.<sup>7</sup> On the basis of the transmission electron microscope (TEM) observation, Lee et al.<sup>14</sup> observed lattice modulation (dark stripes) in tensile LCO films, and believed that they are the origin of magnetism. This conclusion is consistent with the results of ab initio calculations.<sup>15</sup> However, Biškup et al.<sup>16</sup> declared that oxygen vacancy superstructure will be formed in the LCO films, which is responsible for the FM order. Recently, Lan et al.<sup>17</sup> established a close relation between saturation magnetization and the density of dark stripes in the La<sub>1-x</sub>Sr<sub>x</sub>CoO<sub>3</sub> films, suggesting the importance of lattice modulation on FM order rather than oxygen vacancy. There are also suggestions that both oxygen vacancy and lattice strain are indispensable for

magnetism.<sup>18</sup> Recently, we found that the combined effects of Sr-doping and lattice strains can even produce a nonmagnetic window, due to the suppression of superexchange by Sr-doping.<sup>19</sup> Although these opinions on the FM origin are controversial, lattice strains is no doubt an important factor affecting the magnetic properties of the LCO.

In general, lattice strain will be different in the LCO films when film thickness is different, and considerable lattice relaxation will occur in thick films, leading to a magnetic degeneration.<sup>18,19</sup> However, large unreleased strain can be achieved in epitaxial MLs.<sup>20–22</sup> In addition to this, interlayer coupling can also be introduced to the MLs, expanding the space for material exploration.<sup>23–28</sup> As recently reported,<sup>29</sup> a *d*-orbital reconstruction from the  $t_{2g}^{6-\delta}e_g^\delta$  state to the  $t_{2g}^6$  state has been induced by the decrease in dimensionality for the LCO/LaAlO<sub>3</sub> (LAO) multilayers grown on NdGaO<sub>3</sub>.

In this paper, we performed a systematic study on the structural and magnetic properties of LCO/STO MLs grown on different substrates, where each LCO layer is sandwiched between two STO layers to be fully strained. We found that the magnetic order of the MLs is enhanced considerably compared with corresponding LCO single layer (SL). For example, the magnetization vanishes when film thickness is below ~6 nm for a LCO SL grown on STO, whereas it remains significant down to the layer thickness of ~1.5 nm for the LCO in MLs. This

Received: March 30, 2016

Accepted: July 5, 2016

Published: July 5, 2016

result is consistent with our TEM analysis, according to which lattice modulation is significant in the MLs while it becomes vague in thin LCO films.

## 2. EXPERIMENTAL SECTION

Multilayers comprising alternatively stacked LCO and STO layers were grown, by the pulsed laser ablation technique from ceramic targets, on (100)-orientated LAO,  $\text{Sr}_{0.7}\text{La}_{0.3}\text{Al}_{0.65}\text{Ta}_{0.35}\text{O}_3$  (LSAT), and STO substrates ( $3 \times 5 \times 0.5 \text{ mm}^3$ ). During the deposition, the substrate temperature was maintained at  $750 \text{ }^\circ\text{C}$  and the oxygen pressure was fixed to 50 Pa. After deposition, the samples were furnace-cooled to room temperature in an oxygen atmosphere of 100 Pa. The layer thickness of LCO was set to a value between  $d = 1.4$  and  $9.8 \text{ nm}$ , while the STO layer thickness was fixed to  $4 \text{ nm}$ . The total thickness of the multilayer is  $t = 4(n + 1) + nd$  in the unit of nanometer, where  $n$  and  $n + 1$  are the numbers of the STO and LCO layers, respectively. In this work,  $n$  has been set to 3, 4, 6, 7, and 9, corresponding to the LCO layer thickness of  $d = 9.8, 7, 4.2, 2.8,$  and  $1.4 \text{ nm}$ , respectively. Here  $n$  and  $d$  were chosen so that the total thickness of the MLs varies around  $50 \text{ nm}$ . Hereafter, the MLs will be denoted as  $\text{LCO}(d)/\text{STO}$ .

Surface morphology of the MLs was measured by atomic force microscope (AFM, SPI 3800N, Seiko). Crystal structure of the films was analyzed at room temperature by a Bruker diffractometer (D8 Discover,  $\text{Cu K}\alpha$  radiation). Lattice images were acquired by a high-resolution aberration-corrected scanning TEM with double  $\text{C}_s$  correctors for the condenser lens and objective lens (STEM, JEM-ARM200F). Magnetic measurements were conducted by a superconducting quantum interference device (VSM-SQUID) magnetometer.

## 3. RESULTS AND DISCUSSION

Figure 1a is a schematic diagram of the LCO/STO MLs. The LCO and STO layers are alternatively stacked, with the bottom

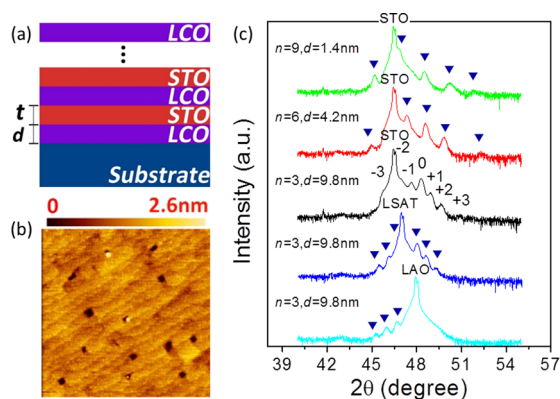


**Figure 1.** (a) Schematic picture of the stacking order of LCO and STO in the multilayer films. (b) AFM image for  $2n + 1 = 13$ ,  $d = 4.2 \text{ nm}$  on STO. Image size is  $1 \mu\text{m} \times 1 \mu\text{m}$ . (c) X-ray diffraction  $\theta$ - $2\theta$  scan around the  $\text{LaCoO}_3$  (002) reflection.

and the top layers being LCO. Figure 1b shows the topography for the typical ML of  $\text{LCO}(d)/\text{STO}$  grown on STO ( $d = 4.2 \text{ nm}$ ). Terrace-structured surface morphology, with a step height of  $\sim 4 \text{ \AA}$ , can be clearly seen, indicating a layer-by-layer growth of the film. Figure 1c presents the representative X-ray diffraction spectra for selected MLs. The clear satellite peaks around the main (002) peak are a typical feature of the MLs. The appearance of the satellite peaks with the indices up to 3 reveals the high quality of the MLs. Satellite peaks are also observed in the MLs on LAO, though the film-substrate lattice mismatch is large in this case.

According to the schematic diagram in Figure 2a, the lattice mismatches between LCO and LAO, LSAT, and STO can be

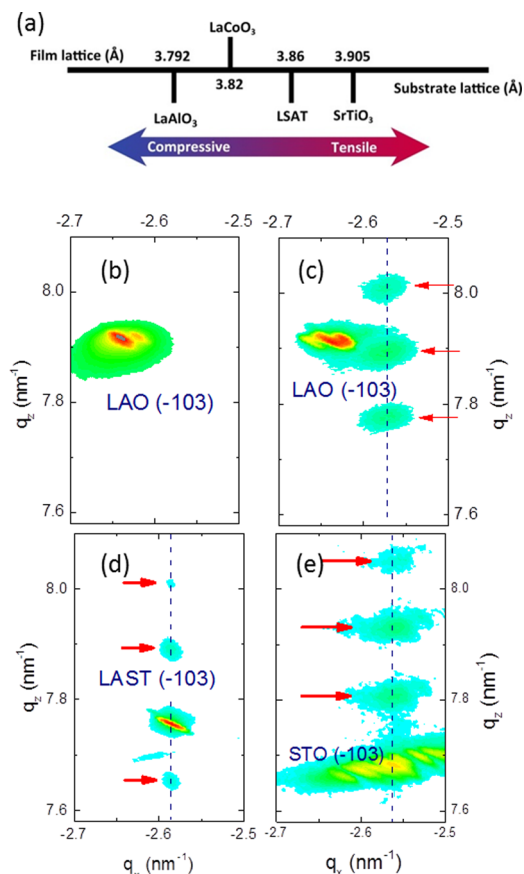


**Figure 2.** (a) Schematic diagram comparing the lattice constants of LCO and LAO, LSAT, and STO. Reciprocal space map of the (103) reflection for the LCO/STO films with  $d = 7 \text{ nm}$  on LAO (b), and  $d = 4.2 \text{ nm}$  on LAO (c), LSAT (d), and STO (e).

calculated, and they are  $-0.73\%$ ,  $1.05\%$ , and  $2.23\%$ , respectively. This implies that the lattice strain is compressive for the LCO films above LAO and tensile above LSAT and STO. To get the information on in-plane lattice constants, the reciprocal space mapping (RSM) of the (103) reflection is measured. Figures 2c, d, and e show the typical results of the  $\text{LCO}(d)/\text{STO}$  MLs with  $d = 4.2 \text{ nm}$ , grown on LAO, LSAT, and STO, respectively. As expected, clear satellite peaks are observed besides the main (103) reflection. Remarkably, the diffraction peaks of the two MLs on LSAT and STO align vertically with those of the substrates, indicating exactly the same in-plane lattice constant for the film with substrates. In contrast, the reflections of the MLs above LAO display an obvious misalignment with those of the substrate, right-shifting along  $x$ -axis. Further analysis shows that the in-plane lattice parameter is  $\sim 3.886 \text{ \AA}$ , significantly greater than that of LAO. Obviously, due to large lattice mismatch, the  $\text{LCO}(d)/\text{STO}$  ML on LAO takes a lattice constant close to STO instead of LAO. However, by increasing the LCO layer up to  $7 \text{ nm}$ , the multilayer on LAO demonstrates a RSM with graded relaxation, without satellite peaks (Figure 2b). The average in-plane lattice constant remains compressive, and the average out-of-plane lattice constant is close to LAO. This coincides with the previous XRD spectrum.

From the RSM of the MLs, the average in-plane ( $a$ ) and out-of-plane ( $c$ ) lattice parameters can be deduced, and are presented in Figure 3 as functions of the layer thickness of

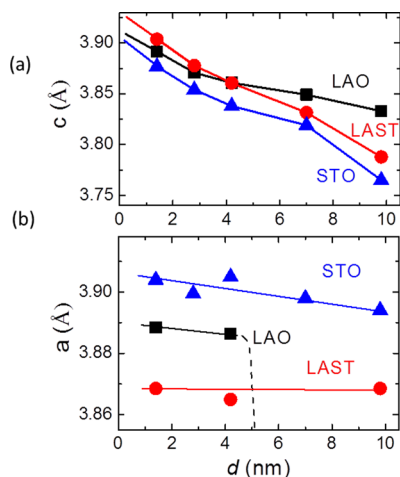


**Figure 3.** Out-of-plane (a) and in-plane (b) lattice parameters as functions of  $d$ , deduced from the RSM.

LCO.  $c$  exhibits a monotonic increase with the decrease of the layer thickness of LCO, approaching the values of 3.90, 3.91, and 3.93 Å as  $d \rightarrow 0$ , for the MLs on STO, LSAT, and LAO, respectively. All the MLs on LSAT and STO are fully strained, showing the same in-plane lattice parameters with substrates. This implies a tensile strain in the LCO layer. However, strain relaxation takes place for the MLs on LAO when  $d \leq 4.2$  nm. Possibly, the large lattice mismatch between STO and LAO causes an incoherent film growth when the LCO layer is thin (in this case the film MLs are mainly composed of STO): misfit dislocations could be formed in the STO layer<sup>30</sup> and the strain is fully relaxed, resulting in an in-plane lattice parameter considerably larger than that of LAO. However, when  $d$  exceeds 7 nm, in-plane lattice constant of the MLs falls abruptly and the out-of-plane lattice constant rises abnormally. In the meantime, a diffusive diffraction peak appears in the RSM, and the satellite peaks disappear (Figure 2b). A possible explanation is that the in-plane lattice shrinks when LCO is thick, leading to gradient strain relaxations.

As reported, dark stripes perpendicular to interface will appear in tensile LCO films, accompanying the occurrence of FM order.<sup>15–19</sup> To obtain further information about lattice strains and microscopic structure of the MLs, a STEM analysis of the MLs has been performed. Figure 4a shows high-angle

annular dark field (HAADF) images of the cross section of the LCO(7)/STO MLs grown on STO. From these images it is confirmed that the LCO and STO layers are continuous and flat. Figure 4b is a close view of the HAADF image near the middle of the MLs. The bright and dark regions correspond to LCO and STO, respectively. Dark stripes perpendicular to interface are observed in the LCO layer, appearing every other three or four columns. The longest stripes are only 2–3 unit cells away from the interface, similar to what is observed in thick LCO SLs. As shown in Figure 4b, dark stripes exhibit a large in-plane lattice constant. This explains why they prefer to appear in tensile LCO films. However, for a thin LCO single film that has the same thickness as the LCO layer in the MLs, structural modulation is not obvious, and dark stripes are nearly invisible (Figure 4c). In a thin LCO film grown on STO structural modulation is depressed since the film is fully strained. In the MLs, the LCO and STO layers are intercalated in sequence. In this case, interlayer diffusion and interfacial roughness are inevitable, as evidenced by the HAADF image (Figure 4b) and the results of electron energy loss spectroscopy (EELS) analysis (not shown). As a consequence, the LCO layer may be not uniformly strained, resulting in dark stripes with large unit cells even when the LCO layer is thin. We also observed dark stripes in the MLs on LAO, though these stripes are parallel to interface (Supporting Information Figure S1). This is understandable since the compressive strains in this kind of MLs make the out-of-plane lattice constant expanded.

To reveal the relation between lattice strain and magnetism, the magnetization of the LCO SL and the MLs was measured. In Figure 5a we show the magnetization of the LCO/STO films as a function of temperature ( $M-T$ ), measured in the field-cooling mode under an applied field of 0.05 T. The magnetic field-dependent magnetizations ( $M-H$ ) measured at 10 K are shown in Figure 5b. The tensile LCO films are in the FM state at low temperatures, similar to previous reports.<sup>6–8,14,15</sup> With the decrease of film thickness, the FM order is weakened. These are phenomena similar to those observed in manganite films.<sup>31,32</sup> Lattice strains and defects at interface/surface depress the magnetic exchange between magnetic ions. According to Figure 5c, both the Curie temperature and saturation magnetization vary slightly as film thickness changes from 50 to 10 nm, but drop rapidly for further decrease in film thickness. By extrapolating the  $M_s-d$  relation to  $M_s \rightarrow 0$ , a magnetic dead layer can be deduced, and it is  $\sim 5$  nm in thickness for the LCO SLs (inset in Figure 5c). As well established, in the tensile LCO films, the magnetic interaction is the superexchange between the HS–LS–HS  $\text{Co}^{3+}$  ions via intermediate oxygen anions. In ultrathin LCO films, the dark

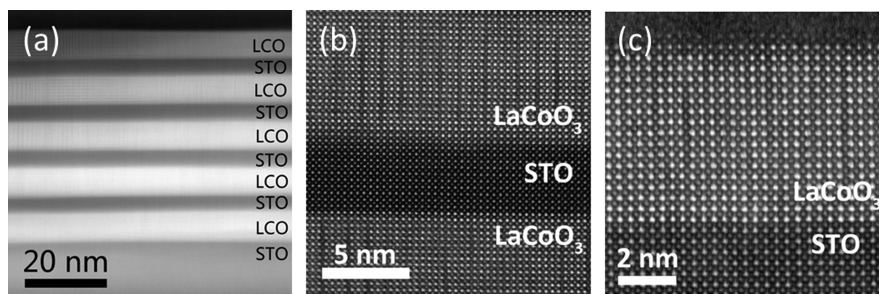


**Figure 4.** (a) and (b) High-angle annular dark-field (HAADF) image of the LCO/STO multilayers on STO with  $d = 7$  nm. (c) HAADF image of a 7 nm-thick LCO film on STO. Periodical dark stripes perpendicular to interface can be clearly seen in the LCO/STO multilayers but cannot in the LCO single layer.

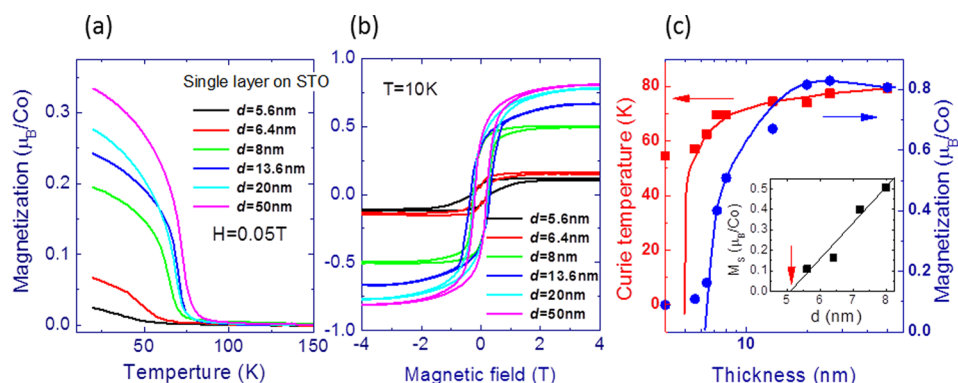


**Figure 5.** (a) Temperature-dependent magnetization of the LCO single layer film on STO, recorded in the warming process after field cooling the films to 10 K. The applied field is 0.05 T (b). Isothermal magnetizations of the film, recorded at 10 K. (c) Curie temperature and saturation magnetization as a function of  $d$ , extracted from the  $M$ - $T$  and  $M$ - $H$  curves in (a) and (b), respectively. Inset plot shows the saturation magnetization as a function of layer thickness of LCO in the MLs. Arrow indicates the thickness of magnetic dead layer.

stripes are not clear, which means a low content of HS  $\text{Co}^{3+}$  ions. As a result, the magnetic exchange is weakened.

In Figure 6a we show the typical magnetization of the MLs as a function of temperature, also measured in the field-cooling mode with a field of 0.05 T. Figure 6b shows the magnetic field-dependent magnetizations measured at 10 K. At first glance, both the  $M$ - $T$  and  $M$ - $H$  curves of the MLs are very similar to those of the LCO SLs: the magnetic order weakens gradually with the decrease of the LCO layer thickness. However, a careful analysis reveals the difference between the MLs and the LCO SLs. As shown in Figures 6c and d, either the Curie temperature or the saturation magnetization is obviously larger for the former than for the latter when the layer thickness of LCO is similar. For example, the  $T_C$  can be clearly identified for the MLs with the LCO layer down to 1.4 nm, whereas it disappears below 5.6 nm for the LCO SL (Figure 6e). Also, the  $M_S$ - $d$  curves of the MLs show a left shift compared with those of the LCO SL, i.e., the FM order persists when the LCO layer is ultrathin for the MLs (Figure 6f). The difference of the MLs and LCO SLs has been highlighted by green in Figures 6e and f. Different from the SLs, the compressive LCO/STO ML grown on LAO exhibits the typical FM behavior. For  $d = 9.7$  252 nm film, the saturation magnetization is  $0.44 \mu_B/\text{Co}$ . This value is much larger than that of the SL on LAO. This change in  $M_s$  is closely related to the variation in lattice constant  $c$ .

To trace the effect of the STO interlayer, we also studied the magnetic behaviors of the MLs with a STO layer of 1 nm but different LCO layers. In Figure 7 we summarize the saturation magnetization, deduced from the magnetic field dependence of the magnetization, for the LCO( $d$ )/STO(4), LCO( $d$ )/STO(1) MLs, and the LCO SLs. Interestingly, the LCO( $d$ )/STO(1) MLs display the highest  $M_S$  while the LCO SL shows the lowest  $M_S$ . This means that a STO interlayer of 1 nm is enough to enhance the FM order in the MLs. A simple analysis shows that the magnetic dead layer is absent in LCO( $d$ )/STO(1) and  $\sim 0.5$  nm in the LCO( $d$ )/STO(4), which is much thinner than that in the LCO SL ( $\sim 5$  nm).

Different from the SLs, the compressive LCO/STO ML grown on LAO exhibits the typical FM behavior. For  $d = 9.7$  nm film, the saturation moment  $M_s$  is  $0.44 \mu_B/\text{Co}$ . This value is much larger than that of the SL on LAO. This changing in  $M_s$  is closely related to the changing in lattice constant  $c$ .

There are two possible origins for the enhanced magnetism in the MLs. The first one is the full lattice strains maintained by the STO interlayer. According to our experiments, obvious

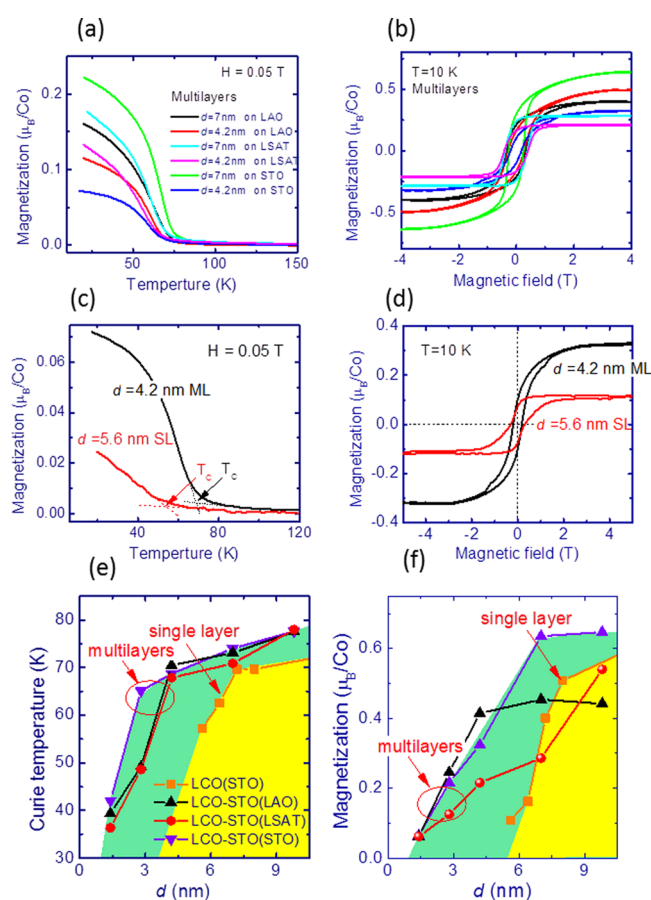


**Figure 6.** (a) Temperature-dependent magnetizations and (b) isothermal magnetizations of the multilayers and single-layer LCO films, measured in the field-cooling mode under an applied field of 0.05 T for (a) and at a temperature of 10 K for (b). (c) Comparison of the  $M$ - $T$  relation for the LCO single layer and the LCO/STO multilayer. Arrows here indicate the determination of the Curie temperature. (d) Corresponding  $M$ - $H$  curves for the above two samples, measured at the temperature of 10 K. The data in (c) and (d) show the magnetic enhancement for the ML. Curie temperature (e) and saturation magnetization (f) as functions of the layer thickness of LCO ( $d$ ) in the LCO/STO multilayers, extracted from the  $M$ - $T$  and  $M$ - $H$  curves, respectively. The  $T_C$  and  $M_S$  for the LCO single layer are also presented for comparison.

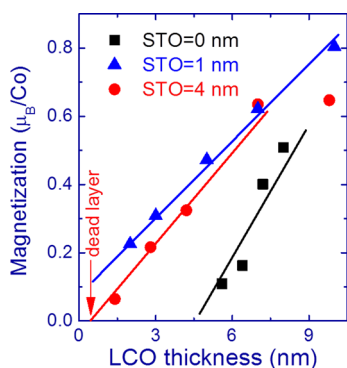


**Figure 7.** Saturation magnetizations as functions of the layer thickness of LCO in the LCO/STO multilayers with the STO layer thickness of 0, 1, and 4 nm, respectively. Solid lines are guides for the eye. Arrow marks the dead layer for one set of the MLs.

strain relaxation occurs when layer thickness is above 40 nm for tensile LCO films. Although the thickness of the MLs studied here varies from 45.4 to 53.2 nm, the total thickness of the LCO layer in the MLs ranges from 12.6 to 29.4 nm. This means that the large lattice strains may not be the main reason for the enhanced magnetism observed here. The second origin may be the inlayer coupling that leads to a structural modulation that supports magnetism. From the HAADF images in Figure 4b for the MLs and Figure 4c for the LCO SL, we get the conclusion that dark stripes with large in-plane lattice constants prefer to appear in the MLs, i.e., the LCO layer is easily modulated when it is sandwiched by two STO layers. The reason is still not very clear at present. According to the EELS analysis (not shown), there is an interface layer ( $\sim 1$  nm thick) where both Co and Ti are detected. This may have something to do with the structural modulation in the ultrathin LCO layer of the MLs. Fascinatingly, this interface layer is absent between the LCO film and the STO substrate. It has been well established that the structural modulation will cause a LS to HS transition for the  $\text{Co}^{3+}$  ions, resulting in the HS–LS–HS superexchange.

#### 4. CONCLUSION

In summary, the structural and magnetic properties of the LCO/STO MLs have been systematically studied. It is found that the insertion of the STO intermediate layer has significantly enhanced the magnetic order of the LCO layer, as demonstrated by the increase of the Curie temperature and the saturation magnetization compared with those of the single LCO layer. A definite ferromagnetic order can be observed in the ML with the LCO layer of  $\sim 1.4$  nm whereas it vanishes below  $\sim 6$  nm for the LCO SL. We observed signatures for the preferred formation of dark stripes, which are believed to be the origin for the magnetic order, in the MLs than in the SLs. The present work reveals the importance of interlayer coupling, and suggests a feasible approach to tune the magnetism in perovskite oxide films.

#### ■ ASSOCIATED CONTENT

##### Supporting Information

The Supporting Information is available free of charge on the ACS Publications website at DOI: 10.1021/acsami.6b03756.

Additional data on lattice image for the multilayers films grown on  $\text{LaAlO}_3$  (PDF)

#### ■ AUTHOR INFORMATION

##### Corresponding Author

\*E-mail: jrsun@iphy.ac.cn.

##### Author Contributions

J. R.S. conceived and designed the experiments, and analyzed and interpreted the data. H.R.Z. prepared the samples, performed the structural and magnetic measurements, and together with H.W.Y., D.S.H., and S.F.W., primarily analyzed the experimental data. The AFM characterizations of the sample were made by J.Z. and T.K. Transmission electron microscope analysis was conducted by X.S., Q.Q.L., and R.C.Y. The manuscript was written by H.R.Z. and J.R.S. B.G.S. oversaw the project. All authors commented on the manuscript.

##### Notes

The authors declare no competing financial interest.

#### ■ ACKNOWLEDGMENTS

This work has been supported by the National Basic Research of China (Grants 2016YFA0300701, 2012CB921403, and 2013CB921701) and the National Natural Science Foundation of China (Grants 11520101002, 11074285, 51372064, and 11134007).

#### ■ REFERENCES

- (1) Lemeé, N.; Infante, I. C.; Hubault, C.; Boule, A.; Blanc, N.; Boudet, N.; Demange, V.; Karkut, M. G. Polarization Rotation in Ferroelectric Tricolor  $\text{PbTiO}_3/\text{SrTiO}_3/\text{PbZr}_{0.2}\text{Ti}_{0.8}\text{O}_3$  Superlattices. *ACS Appl. Mater. Interfaces* **2015**, *7*, 19906–19913.
- (2) Moshnyaga, V.; Damaschke, B.; Shapoval, O.; Belenchuk, A.; Faupel, J.; Lebedev, O. I.; Verbeeck, J.; van Tendeloo, G.; Mücksch, M.; Tsurkan, V.; Tidecks, R.; Samwer, K. Structural Phase Transition at the Percolation Threshold in Epitaxial  $(\text{La}_{0.7}\text{Ca}_{0.3}\text{MnO}_3)_{1-x}(\text{MgO})_x$  Nanocomposite Films. *Nat. Mater.* **2003**, *2*, 247–252.
- (3) Lee, J. H.; Fang, L.; Vlahos, E.; Ke, X.; Jung, Y. W.; Kourkoutis, L. F.; Kim, J.; Ryan, P. J.; Heeg, T.; Roeckerath, M.; Goian, V.; Bernhagen, M.; Uecker, R.; Hammel, P. C.; Rabe, K. M.; Kamba, S.; Schubert, J.; Freeland, J. W.; Muller, D. A.; Fennie, C. J.; Schiffer, P.; Gopalan, V.; Johnston-Halperin, E.; Schlom, D. G. A Strong Ferroelectric Ferromagnet Created by Means of Spin-Lattice Coupling. *Nature* **2010**, *466*, 954–958.
- (4) Catalan, G.; Lubk, A.; Vlooswijk, A. H. G.; Snoeck, E.; Magen, C.; Janssens, A.; Rispens, G.; Rijnders, G.; Blank, D. H. A.; Noheda, B. Flexoelectric Rotation of Polarization in Ferroelectric Thin Films. *Nat. Mater.* **2011**, *10*, 963–967.
- (5) Lin, Q.; Wang, D.; Chen, Z.; Liu, W.; Lim, S.; Li, S. Periodicity Dependence of the Built-In Electric Field in  $(\text{Ba}_{0.7}\text{Ca}_{0.3})\text{TiO}_3/\text{Ba}(\text{Zr}_{0.2}\text{Ti}_{0.8})\text{O}_3$  Ferroelectric Superlattices. *ACS Appl. Mater. Interfaces* **2015**, *7*, 26301–26306.
- (6) Fuchs, D.; Pinta, C.; Schwarz, T.; Schweiss, P.; Nagel, P.; Schuppler, S.; Schneider, R.; Merz, M.; Roth, G.; v Löhneysen, H. Ferromagnetic Order in Epitaxially Strained  $\text{LaCoO}_3$  Thin Films. *Phys. Rev. B: Condens. Matter Mater. Phys.* **2007**, *75*, No. 144402.
- (7) Fuchs, D.; Arac, E.; Pinta, C.; Schuppler, S.; Schneider, R.; v Löhneysen, H. Tuning the Magnetic Properties of  $\text{LaCoO}_3$  Thin Films by Epitaxial Strain. *Phys. Rev. B: Condens. Matter Mater. Phys.* **2008**, *77*, No. 014434.
- (8) Fuchs, D.; Dieterle, L.; Arac, E.; Eder, R.; Adelman, P.; Eyert, V.; Kopp, T.; Schneider, R.; Gerthsen, D.; v Löhneysen, H. Suppression of the Ferromagnetic State in  $\text{LaCoO}_3$  Films by Rhombohedral Distortion. *Phys. Rev. B: Condens. Matter Mater. Phys.* **2009**, *79*, No. 024424.
- (9) Seo, H.; Posadas, A.; Demkov, A. A. Strain-Driven Spin-State Transition and Superexchange Interaction in  $\text{LaCoO}_3$ : *Ab initio* Study. *Phys. Rev. B: Condens. Matter Mater. Phys.* **2012**, *86*, No. 014430.
- (10) Itoh, M.; Natori, I.; Kubota, S.; Motoya, K. Spin-glass Behavior and Magnetic Phase Diagram of  $\text{La}_{1-x}\text{Sr}_x\text{CoO}_3$  ( $0 \leq x \leq 0.5$ ) Studied

by Magnetization Measurements. *J. Phys. Soc. Jpn.* **1994**, *63*, 1486–1493.

(11) Tokura, Y.; Okimoto, Y.; Yamaguchi, S.; Taniguchi, H.; Kimura, T.; Takagi, H. Thermally Induced Insulator-Metal Transition in  $\text{LaCoO}_3$ : A View Based on the Mott Transition. *Phys. Rev. B: Condens. Matter Mater. Phys.* **1995**, *58*, 1699–1702.

(12) Saitoh, T.; Mizokawa, T.; Fujimori, A.; Abbate, M.; Takeda, Y.; Takano, M. Electronic Structure and Temperature-Induced Paramagnetism in  $\text{LaCoO}_3$ . *Phys. Rev. B: Condens. Matter Mater. Phys.* **1997**, *55*, 4257–4266.

(13) Caciuffo, R.; Rinaldi, D.; Barucca, G. L.; Mira, J.; Rivas, J.; Señaris-Rodríguez, M. A.; Radaelli, P. G.; Fiorani, D.; Goodenough, J. B. Structural Details and Magnetic Order of  $\text{La}_{1-x}\text{Sr}_x\text{CoO}_3$  ( $x \leq 0.3$ ). *Phys. Rev. B: Condens. Matter Mater. Phys.* **1999**, *59*, 1068–1078.

(14) Choi, W. S.; Kwon, J. H.; Jeon, H.; Hamann-Borrero, J. E.; Radi, A.; Macke, S.; Sutarro, R.; He, F.; Sawatzky, G. A.; Hinkov, V.; Kim, M.; Lee, H. N. Strain-Induced Spin States in Atomically Ordered Cobaltites. *Nano Lett.* **2012**, *12*, 4966–4970.

(15) Kwon, J. H.; Choi, W. S.; Kwon, Y. K.; Jung, R.; Zuo, J. M.; Lee, H. N.; Kim, M. Nanoscale Spin-State Ordering in  $\text{LaCoO}_3$  Epitaxial Thin Films. *Chem. Mater.* **2014**, *26*, 2496–2501.

(16) Biškup, N.; Salafranca, J.; Mehta, V.; Oxley, M. P.; Suzuki, Y.; Pennycook, S. J.; Pantelides, S. T.; Varela, M. Insulating Ferromagnetic  $\text{LaCoO}_{3-\delta}$  Films: a Phase Induced by Ordering of Oxygen Vacancies. *Phys. Rev. Lett.* **2014**, *112*, No. 087202.

(17) Lan, Q. Q.; Shen, X.; Yang, H. W.; Zhang, H. R.; Zhang, J.; Guan, X. X.; Yao, Y.; Wang, Y. G.; Yu, R. C.; Peng, Y.; Sun, J. R. Correlation Between Magnetism and “Dark Stripes” in Strained  $\text{La}_{1-x}\text{Sr}_x\text{CoO}_3$  Epitaxial Films ( $0 \leq x \leq 0.1$ ). *Appl. Phys. Lett.* **2015**, *107*, 242404.

(18) Mehta, V. V.; Biskup, N.; Jenkins, C.; Arenholz, E.; Varela, M.; Suzuki, Y. Long-Range Ferromagnetic Order in  $\text{LaCoO}_{3-\delta}$  Epitaxial Films Due to the Interplay of Epitaxial Strain and Oxygen Vacancy Ordering. *Phys. Rev. B: Condens. Matter Mater. Phys.* **2015**, *91*, No. 144418.

(19) Yang, H. W.; Zhang, H. R.; Li, Y.; Wang, S. F.; Shen, X.; Lan, Q. Q.; Meng, S.; Yu, R. C.; Shen, B. G.; Sun, J. R. Anomalous Magnetism in Strained  $\text{La}_{1-x}\text{Sr}_x\text{CoO}_3$  Epitaxial Films ( $0 \leq x \leq 0.5$ ). *Sci. Rep.* **2014**, *4*, 6206.

(20) Liang, Y. C.; Wu, T. B.; Lee, H. Y.; Hsieh, Y. W. Structural Characteristics of Epitaxial  $\text{BaTiO}_3/\text{LaNiO}_3$  Superlattice. *J. Appl. Phys.* **2004**, *96*, 584–589.

(21) Jaakola, I.; Levoska, J.; Tyunina, M. Multilayers and Superlattices of Ferroelectric Barium Strontium Titanate. *J. Appl. Phys.* **2007**, *102*, 4108.

(22) Narkilahti, J.; Plekh, M.; Levoska, J.; Tyunina, M. Anomalous Growth and Properties of  $\text{SrTiO}_3\text{-NaNbO}_3$  Superlattices. *Phys. Rev. B: Condens. Matter Mater. Phys.* **2009**, *79*, No. 014106.

(23) Choi, W. S.; Jeong, D. W.; Seo, S. S. A.; Lee, Y. S.; Kim, T. H.; Jang, S. Y.; Lee, H. N.; Myung-Whun, K. Charge States and Magnetic Ordering in  $\text{LaMnO}_3/\text{SrTiO}_3$  Superlattices. *Phys. Rev. B: Condens. Matter Mater. Phys.* **2011**, *83*, No. 195113.

(24) Hoffman, J.; Tung, I. C.; Nelson-Cheeseman, B. B.; Liu, M.; Freeland, J. W.; Bhattacharya, A. Charge Transfer and Interfacial Magnetism in  $(\text{LaNiO}_3)_n/(\text{LaMnO}_3)_2$  Superlattices. *Phys. Rev. B: Condens. Matter Mater. Phys.* **2013**, *88*, No. 144411.

(25) Das, S.; Sen, K.; Marozau, I.; Uribe-Laverde, M. A.; Biskup, N.; Varela, M.; Khaydukov, Y.; Soltwedel, O.; Keller, T.; Döbeli, M.; Schneider, C. W.; Bernhard, C. Structural, Magnetic, and Superconducting Properties of Pulsed-Laser-Deposition-Grown  $\text{La}_{1.85}\text{Sr}_{0.15}\text{CuO}_4/\text{La}_{2/3}\text{Ca}_{1/3}\text{MnO}_3$  Superlattices on (001)-Oriented  $\text{LaSrAlO}_4$  Substrates. *Phys. Rev. B: Condens. Matter Mater. Phys.* **2014**, *89*, No. 094511.

(26) Grutter, A. J.; Yang, H.; Kirby, B. J.; Fitzsimmons, M. R.; Aguiar, J. A.; Browning, N. D.; Jenkins, C. A.; Arenholz, E.; Mehta, V. V.; Alaan, U. S.; Suzuki, Y. Interfacial Ferromagnetism in  $\text{LaNiO}_3/\text{CaMnO}_3$  Superlattices. *Phys. Rev. Lett.* **2013**, *111*, No. 087202.

(27) Garcia-Barriocanal, J.; Bruno, F. Y.; Rivera-Calzada, A.; Sefrioui, Z.; Nemes, N. M.; Garcia-Hernández, M.; Rubio-Zuazo, J.; Castro, G.

R.; Varela, M.; Pennycook, S. J.; Leon, C.; Santamaria, J. Charge Leakage” at  $\text{LaMnO}_3/\text{SrTiO}_3$  Interfaces. *Adv. Mater.* **2010**, *22*, 627–632.

(28) Zhai, X.; Cheng, L.; Liu, Y.; Schlepütz, C. M.; Dong, S.; Li, H.; Zhang, X.; Chu, S.; Zheng, L.; Zhang, J.; Zhao, A.; Hong, H.; Bhattacharya, A.; Eckstein, J. N.; Zeng, C. Correlating Interfacial Octahedral Rotations with Magnetism in  $(\text{LaMnO}_{3+\delta})_N/(\text{SrTiO}_3)_N$  Superlattices. *Nat. Commun.* **2014**, *5*, 4283.

(29) Choi, W. S.; Okamoto, S.; Kim, J. Y.; Kim, K. W.; Moon, S. J.; Cho, D. Y.; Lee, H. N.; Noh, T. W.; Jeong, D. W. Dimensionality Control of *d*-Orbital Occupation in Oxide Superlattices. *Sci. Rep.* **2014**, *4*, 6124.

(30) Das, S.; Herklotz, A.; Pippel, E.; Guo, E. J.; Rata, D.; Dörr, K. Strain Dependence of Antiferromagnetic Interface Coupling in  $\text{La}_{0.7}\text{Sr}_{0.3}\text{MnO}_3/\text{SrRuO}_3$  Superlattices. *Phys. Rev. B: Condens. Matter Mater. Phys.* **2015**, *91*, No. 134405.

(31) Xia, J.; Siemons, W.; Koster, G.; Beasley, M. R.; Kapitulnik, A. Critical Thickness for Itinerant Ferromagnetism in Ultrathin Films of  $\text{SrRuO}_3$ . *Phys. Rev. B: Condens. Matter Mater. Phys.* **2009**, *79*, No. 140407.

(32) Huijben, M.; Martin, L. W.; Chu, Y. H.; Holcomb, M. B.; Yu, P.; Rijnders, G.; Blank, D. H. A.; Ramesh, R. Critical Thickness and Orbital Ordering in Ultrathin  $\text{La}_{0.7}\text{Sr}_{0.3}\text{MnO}_3$  Films. *Phys. Rev. B: Condens. Matter Mater. Phys.* **2008**, *78*, No. 094413.